ELSEVIER

Polymer 43 (2002) 4811–4822

polymer

www.elsevier.com/locate/polymer

Crystallinity measurements of polyamides adsorbed as thin films

Tamara Elzein, Maurice Brogly*, Jacques Schultz

Institut de Chimie des Surfaces et Interfaces—CNRS, 15, Rue Jean Starcky, 68057 Mulhouse, France

Received 22 January 2002; received in revised form 18 March 2002; accepted 25 March 2002

Abstract

The crystallinity degree of thin polyamide films (PA66, 610 and 612) spin coated on four types of substrates are estimated. Two original methods based on the analysis of infrared spectra are proposed. The high sensitivity of polarization modulation reflection-absorption spectroscopy for the study of thin polymer films leads to quantitative results. These two methods offer the possibility to estimate the degree of crystallinity by using infrared spectroscopy, independently of any other technique, if the crystallinity degree in the isotropic bulk state is known. Polyamides are spin coated, on the one hand, on inert and highly reflecting gold substrates, and on the other hand, on the same gold substrates grafted with different chemical functionality. Our calculations show a lower crystallinity degree for inert substrate and higher values for functionalized systems with respect to the bulk. These results suggest that the surface chemical grafts not only play the role of nucleation seeds, but also affect the crystalline morphology as seen by atomic force microscopy.

Keywords: Crystallinity; Polyamides; Infrared

1. Introduction

One of the most important characteristics of semi-crystalline polymers is the degree of crystallinity (X_c). Many properties, such as mechanical ones, are influenced by the crystallinity degree of the material. Thus, polymer crystallinity has a special position in the field of polymer science.

Polyamides are semi-crystalline polymers with many industrial employments. Knowing well their characteristics permits to better identify domains where these polymers could satisfy required properties. PA66, 610 and 612 were the subjects of many studies [1–23]. Because they belong to the same class of linear polyamides and since they have many common properties, they were chosen for this systematic study. Many works were concerned in the study of crystallinity degrees, and many techniques [3,24–26] are used for the estimation of this parameter. In contrast, many of these techniques are not well adapted for the study of adsorbed thin film crystallinity due to the extremely low quantity of analyzed matter in the adsorbed state and also due to the sample geometry.

In this present work, we would focus on the estimation of crystallinity degree of PA thin films spin coated on different substrates. The estimation of the *degree of crystallinity* X_c permits to better understand the crystallization and growth phenomenon of the adsorbed system, even if it is necessary to distinguish between this measured quantity X_c and the degree of crystallization, defined as the time and temperature dependent ratio of the crystallized mass to the original polymer mass [27,28].

Many techniques, such as differential scanning calorimetry (DSC) and infrared spectroscopy in attenuated total reflection (ATR) mode, reflection absorption mode (IRRAS), polarization modulation IRRAS (PM-IRRAS), and atomic force microscopy (AFM), were used to reach our aim. In this paper, we tried to find an independent infrared method for thin films crystallinity measurements without using a calibration route supported by another technique. The choice of IRRAS and PM-IRRAS spectroscopies was appropriate because of their suitability for the analysis of thin polymer films adsorbed on metallic substrates. It is, moreover, a nondestructive probe that offers a high spectral resolution and excellent sensitivity even in the case of monolayer analysis [29–40].

2. Experimental section

2.1. Materials

Polyamides obtained from Sigma Aldrich Co. as 2–5 nm pellets were used. Their characteristics are listed in Table 1.

* Corresponding author. Tel.: +33-3-89-60-8768; fax: +33-3-89-60-8799.

E-mail address: m.brogly@univ-mulhouse.fr (M. Brogly).

0032-3861/02/$ - see front matter
PII: S0032-3861(02)00239-2

Table 1
Characteristics of polyamides

PA	T_g (°C)	T_f (°C)	T_B (°C)	Solvent
66	45	267	197	Trichloroethanol, phenols, sulfuric acid
610	40	240	180	Trichloroethanol, *m*-cresol
612	46	218	180	Trichloroethanol, *m*-cresol

T_g, T_f, T_B are, respectively, the glass transition, melting and Brill [41] temperatures.

Thin films of PA were spin coated from 5 g/l solutions (in trichloroethanol) on the chosen substrates. Acceleration, velocity and spinning time are, respectively, 10^3 rpm/s, 2500 rpm and 60 s.

Gold substrates were prepared by using glass slides cleaned with ethanol, treated by argon plasma for 3 min at a power of 80 W, and heated at 50 °C for 30 min in a piranha solution. A 90 nm gold (99.99% from Balzers) layer was then coated under vacuum (10^{-7} mbar) after immersion (12 h) in 3-mercaptopropyltriethoxysilane solution (in toluene). 3-Mercaptopropyltriethoxysilane (95%) from ABCR is used as a coupling agent between glass slides and gold coatings.

For grafting (Scheme 1), gold substrates are then cleaned by UV radiation before being immersed in the graft solutions for about 12 h.

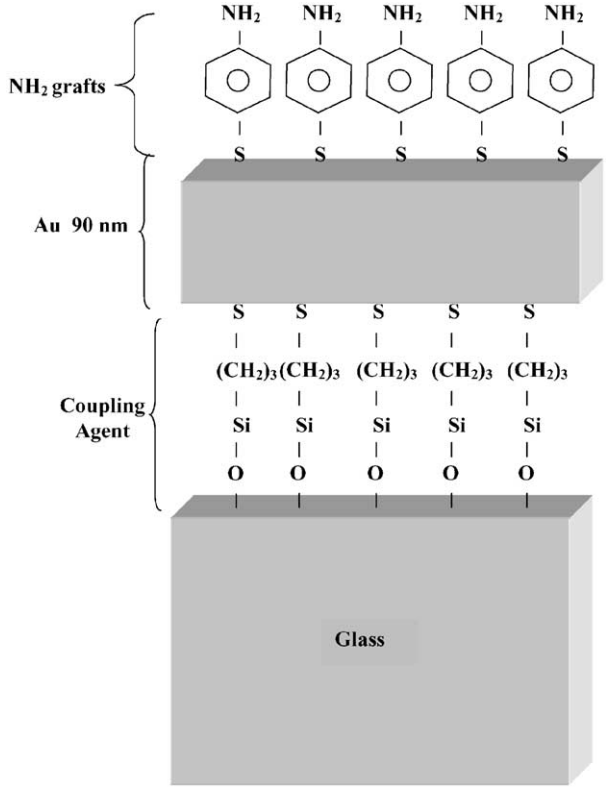

Scheme 1. Representation of NH_2 functionalized substrates.

OH grafts: 11-mercapto-1-undecanol (97% from Sigma Aldrich) solution (in ethanol).
NH_2 grafts: 4-aminothiophenol (90% from Sigma Aldrich) solution (in ethanol).
COOH grafts: thioglycolic acid (99% from Sigma Aldrich) solution (in water).

Typical concentration of 3 mM was chosen for the grafting solutions.

2.2. Differential scanning calorimetry

Thermal analysis of PA bulk pellets was performed with a Mettler TA 4000 differential scanning calorimeter. The sample weight was ranging from 10 to 15 mg. Thermograms were recorded between −30 and 330 °C with a heating rate of 10 °C/min. DSC is used to measure the change in heat capacity of a material under controlled temperature conditions in order to extract many qualitative and quantitative information.

2.3. Infrared spectroscopy

2.3.1. Attenuated total reflection

Bulk polyamides were analyzed by single-reflection ATR infrared spectroscopy. Measurements on polyamide pellets were performed with an IF66S Bruker spectrometer. Spectra were recorded with a mercury–cadmium–telluride (MCT) detector. The number of scans was fixed to 100 with a resolution of 4 cm^{-1}.

2.3.2. Infrared reflection-absorption spectroscopy

Thin films of PA spin coated on gold and functionalized substrates were analyzed by reflection-absorption infrared spectroscopy (IRRAS). Measurements were done with an IFS66 Bruker spectrometer. Spectra were recorded with a MCT detector. Spectra were averaged over 500 scans, with a resolution of 1 cm^{-1}. The angle of the p-polarized incident beam was fixed at 80°.

2.3.3. Polarization-modulation IRRAS

Usually, IRRAS experiments consist in recording the p-polarized reflectivity $R_p(d)$ of the film on a metallic substrate and then normalizing it with respect to that of the bare substrate $R_p(0)$. From these two different experiments, one can compute the so-called IRRAS spectrum $R_p(d)/R_p(0)$.

If the surface layer under study is relatively thick (more than 40 nm), the surface bands appear clearly on the IRRAS spectrum. However, when the sample is an ultra-thin film, the surface detectivity of the IRRAS method is generally not sufficient, and measurement time become very long (several hours). During this period, instabilities in the spectrometer and the detection system may drastically affect the surface spectrum. Moreover, as absorption occurs in the surrounding atmosphere of the sample is also detected, very small changes in these environmental conditions make the surface

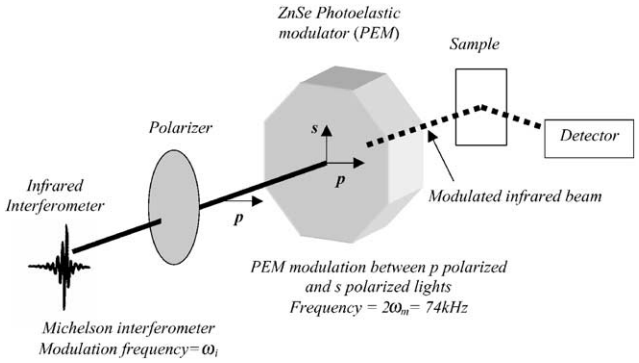

Scheme 2. Optical PM-IRRAS setup.

spectrum less readable. Hence, in situ experiments in a particular IR absorbing atmosphere are generally not possible with IRRAS.

For overcoming the limitations of such an absolute reflectivity R_p measurement, PM-IRRAS was used to study thin films. Thus in PM-IRRAS (Scheme 2), a differential reflectivity ($\Delta R/R$) surface signal is obtained in one step and with all the dynamical range of the detection [42].

Measurements were done with an IF66S Bruker spectrometer, spectra were recorded with a MCT detector, under experimental conditions of 1000 scans, resolution of 1 cm^{-1}, 85° as beam angle of incidence and with a 74 kHz modulation frequency. A ZnSe photoelastic modulator provided by HINDS™ is used.

Briefly, the basic principle of the PM-IRRAS method is to combine the FT-IRRAS experimental conditions with a fast modulation of the polarization state of the incident electric field (ideally between p and s linear states) and to extract, from the detected intensity (using electronic filtering and demodulation), the two signals ($R_p - R_s$) and ($R_p + R_s$) in order to finally compute the differential reflectivity spectrum $\Delta R/R$.

This technique is based on three principles.

- Selection rules induced by the reflection on metallic surface of infrared beam under grazing angles: remembering first that an incident s-polarized light gives no surface electric field and consequently no surface absorption, we can see that PM-IRRAS should be a very efficient way to discriminate near-surface absorption from the isotropic stray absorption occurring farther into the sample environment. Second, that in case of incident p-polarized, the surface electric field of the resulting stationary wave is normal to the metal plane and presents some intensity enhancement due to constructive interferences [42].
- The double modulation of the incident beam: both a Michelson interferometer and a Photo elastic modulator, PEM, modulate infrared radiation from a conventional IR source. The interferometer produces a signal at the detector, which when demodulated is proportional to the total light intensity reflected from the sample surface ($R_p + R_s$). The PEM modulates between the parallel (p) and perpendicular (s) components of the light striking the surface such that after demodulation a signal proportional to the difference in the intensities of the two polarization components ($R_p - R_s$) is obtained. These two signals can be demodulated separately, because there is a large difference in the modulation frequencies of the interferometer and the PEM. The detected intensity is obtained by

$$I_d = \frac{CI_0(\omega_i)}{2}(R_p + R_s - CI_0(\omega_i)(R_p - R_s)J_2(\Phi_0)\cos(2\omega_m t) \quad (1)$$

  where C is the correction factor related to the optical transmission of the setup and the efficiency of the detector; ω_i, the modulation frequency of the interferogram; $2\omega_m$, the modulation frequency of PEM (74 kHz); $I_0(\omega_i)$, the infrared beam intensity (out of the polarizer); $J_2(\Phi_0)$, the second-order Bessel function; Φ_0, the maximal phase change induced by the PEM; R_p and R_s are the parallel and perpendicular reflectivities of the sample, respectively.
- The mathematical treatment of the detected signal in order to obtain the differential reflectivity:

$$\frac{\Delta R}{R} = \frac{R_p - R_s}{R_p + R_s} \quad (2)$$

  The big advantage of this technique is that the two reflectivities R_p and R_s are simultaneously obtained (i.e. during the same experiment) [38–40].

PM-IRRAS selection rules imply that the sign and the intensity of an IR band is a function of the orientation of a transition moment (or functional group) relative to the surface plane. Selection rules are then: if the orientation of a transition moment is parallel to the surface plane then the PM-IRRAS signal is equal to zero. If the orientation is perpendicular to the surface plane then the signal is maximum.

PM-IRRAS technique allows no environmental perturbation on the spectra and high signal to noise ratio. A background spectrum is typically taken to eliminate any instrumental artifacts.

For the spectral decomposition of overlapped bands into individual bands we used the second derivative method performed with the OPUS® software supplied by the spectrometer manufacturer. This software gives also, for each fit, the calculation error, which is minimized.

We used the second derivative method to determine the number and the frequency of overlapped bands. Sharp bands are fitted with a pure lorentzian function, while large ones are a combination of lorentzian and gaussian functions. This latter is the consequence of the multiple lorentzian components summation.

2.4. Ellipsometry

Ellipsometric analyses were performed with a ES4M ellipsometer (Sopra Co.) in order to determine thin film

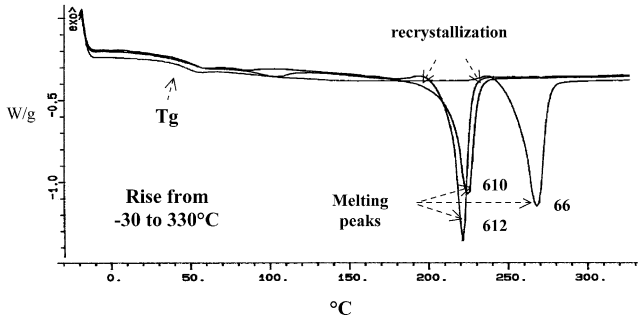

Fig. 1. Thermograms of polyamides 66, 610 and 612.

thickness. Measurements were conducted on thin films coated on silicon wafers. Argon and water plasma, each time for 3 min and 80 W power treated the wafers cleaned with ethanol. Silicon wafers are purchased from Mat Technology as a 280 μm thick plate.

2.5. Atomic force microscopy

Measurements were performed with a Nanoscope IIIa/Dimension 3000 (Digital Instruments) in the tapping mode and under ambient conditions. The electronic extender module allows simultaneously phase detection and height imaging. We used silicon cantilever ($K_c = 40$ N/m and thickness = 125 μm) with a resonant frequency of about 300 kHz. Scan rate is equal to 1 Hz. The free oscillation amplitude A_0 of the oscillating cantilever was around 50 nm, the setpoint amplitude A_{sp} (damped amplitude, when the tip was in intermittent contact) was slightly lower. Topographic (height mode) and rigidity (phase mode) data were recorded simultaneously.

The same samples as those used for IRRAS and PM-IRRAS analysis were prepared for AFM.

3. Results and discussion

3.1. PA bulk analysis

3.1.1. DSC analyses

DSC analyses were carried out to determine the degree of crystallinity of bulk PA pellets. As described in Section 2, thermograms (Fig. 1) were recorded between −30 and 330 °C with a heating rate of 10 °C/min.

These thermograms allow estimating T_g, T_f, ΔH_f and also X_c by using a reference heat of fusion [3] for the 100% crystalline PA66, 610 and 612 equal to 197 J/g (ΔH_{ref}). These values are represented in Table 2.

Table 2
T_g, T_f, ΔH_f and X_c obtained from DSC

PA	T_g (°C)	T_f (°C)	ΔH_f (J/g)	X_c (%)
66	45.4	267	71	36.1
610	44.6	223	66	33.3
612	43.2	220	62	31.2

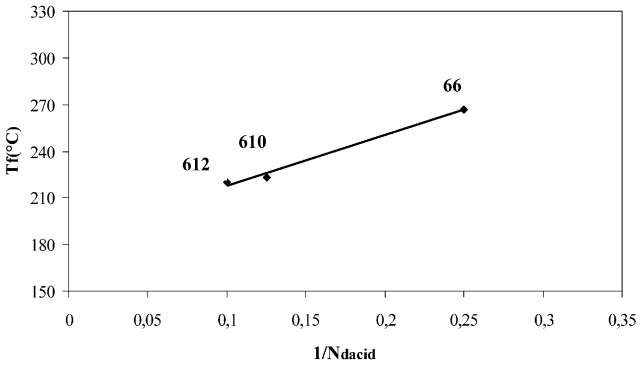

Fig. 2. Evolution of T_f versus the inverse of the carbon number in the aliphatic sequence of the diacid part.

The main parameter that differs from PA66 to 612 is the length of the aliphatic sequence in the diacid part (since they have a common diamine part). The number of aliphatic carbon in the diacid part (N_{diacid}) is equal to 4, 8 and 10, respectively, for PA66, 610 and 612. A linear correlation (Figs. 2 and 3) was found by plotting the melting temperature T_f versus the inverse of N_{diacid}, and X_c versus N_{diacid}.

The crystalline unit cell and lamellae parameters were discussed in many other papers [21–23], and were found to be similar for the 3 PA (except the unit cell *c* parameter). The chain folded lamellae are composed of hydrogen-bonded sheets stacked together through van der Waals interactions. These hydrogen bonds are established between the C=O and NH groups [21–23]. The decrease of the crystallinity degree could be explained by a decrease of the average number of interchain hydrogen bonds caused by the increase of the diacid chain length. The decrease of T_f is related, according to Thompson–Gibbs relationship, to the decrease of the crystalline lamellae thickness.

To better illustrate this argument, a simplified representation of probable H bonds formation is shown in Scheme 3.

This simplified representation (Scheme 3) is useful to explain the decrease of intra and/or interchain probable H-bonds, when the diacid aliphatic chain methylene number increase, due to the increasing distance separating NH and CO groups.

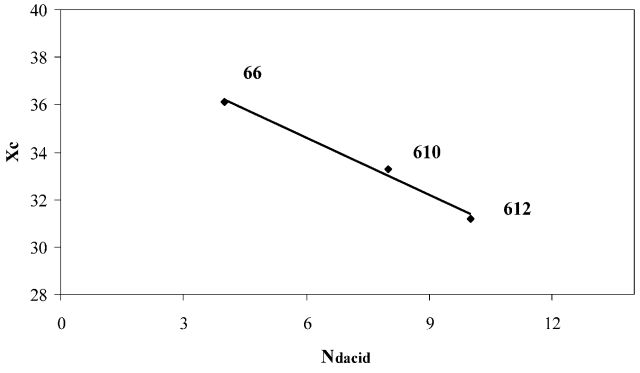

Fig. 3. Evolution of X_c versus the carbon number in the aliphatic sequence of the diacid part.

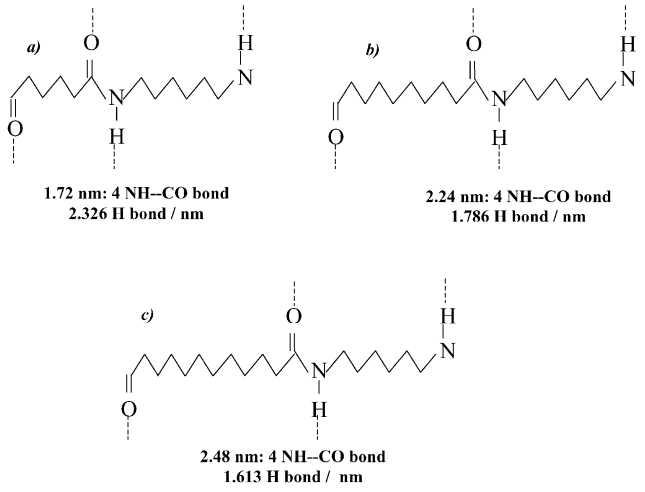

Scheme 3. Simplified representation of probable H bonds formation between NH and C = O groups, with respect to the length of the repetitive unit of (a) PA66, (b) PA610, and (c) PA612

3.1.2. FTIR analyses

PA bulk pellets were analyzed by FTIR spectroscopy in monoreflection ATR mode. Spectra of the 3 PA are shown in Fig. 4.

Many recent studies [3,8] were done on PA66 to give correct assignments of infrared bands. By using many techniques, such as density measurements and infrared spectroscopy, the crystalline and amorphous phase related bands were identified. Some of them were related to the identification of the crystalline structure (triclinic cell) and others can be quantitatively studied for crystallinity degree determination (Table 3).

The most useful bands available to predict crystallinity are the amide ν(C–C=O) stretching bands located at 922 and 936 cm^{-1} attributed, respectively, to the amorphous and the crystalline phases. Due to the specific selection rules of IRRAS and PM-IRRAS for molecular orientation measurements, it is a major importance to choose a functional group representative of both phases. Nevertheless, it is important to note that the signal of vibrators in the amorphous phase is dependent on its anisotropy, which can be affected by the crystalline amount of the global system that could, by a constraint effect, induce an orientation of the amorphous chains, somehow similar to the crystalline one.

Further observation of infrared spectra shows great differences in the 2700–3400 cm^{-1} region (Fig. 4), where the intensity of CH_2 and bonded NH stretching modes are present. The decrease of the crystallinity degree could result in a diminution of bonded NH intensity with respect to the CH_2 one, since that, as mentioned earlier, the crystalline zones are stabilized by hydrogen bonds between NH and CO groups.

Other spectral differences between the 3 PA in 1100–1400 cm^{-1} region are present, but it is difficult to quantify them due, first to the overlapping of many absorption bands, and second to the contribution of specific orientation in the band intensity.

3.2. Quantitative infrared analysis for thin film crystallinity measurement

Crystallinity measurement in thin films is a difficult problem. Moreover, one has to distinguish orientation phenomenon from crystalline organization. Of course,

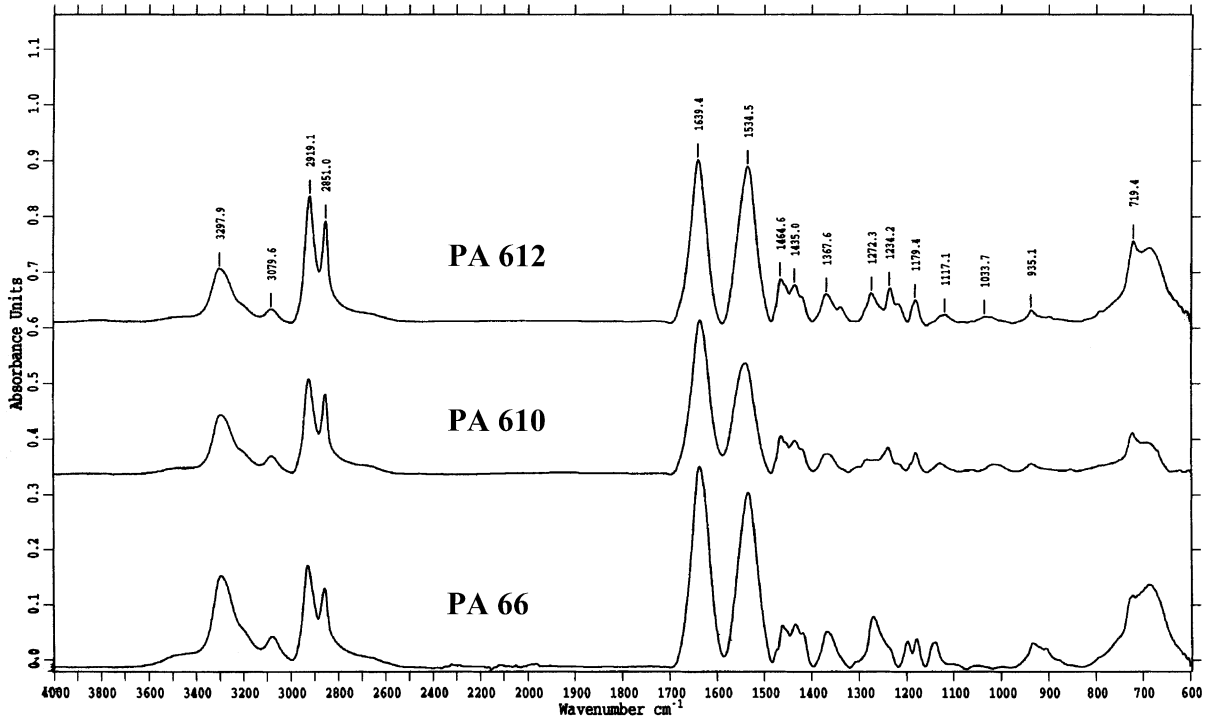

Fig. 4. ATR spectra of PA66, 610 and 612 at room temperature.

Table 3
Crystalline and amorphous characteristic bands of PA

ν (cm^{-1})	Band assignments
900–907	Triclinic structure: amide stretching mode ν(C–C=O) [43]
922	Amorphous phase: amide stretching mode ν(C–C=O) [43]
932–937	Crystalline phase: amide stretching mode ν(C–C=O) [3]
983–987	Triclinic structure: NH rocking mode [8]
1014–1019, 1033–1043 and 1063–1066	Triclinic structure: squeletal stretching ν(C–C) [8]
1128–1136	Amorphous phase: squeletal stretching [8,22]
1140–1146	Partially amorphous: carbonyl twisting mode [8]
1196–1202	Crystalline phase: carbonyl wagging mode [3,8]
1224–1228	Triclinic structure: CH_2 twisting mode coupled with ν(HN–C=O) [43]
1300–1305	Triclinic structure: NH twisting [43]

these two phenomena could be linked. For these reasons, the choice of the vibrators for quantitative calculation is of great importance.

The first possibility is to consider the splitting of the amide stretching modes ν(C–C=O). Two different frequencies are observed, respectively, for the amorphous and for the crystalline phase. The validity of this choice would be discussed later. In case of bulk spectra, these two bands were clearly decomposed and thus, the correlation with the degree of crystallinity was established on the basis of their intensity ratio.

The second possibility is based on the comparison of the absorption band intensities of bonded NH and symmetric CH_2 modes of a single phase. For chains involved in crystalline structures, the choice of symmetric mode is supported by the fact that in these PA chains, the CH_2 symmetric stretching mode vibrate in the same direction than for the bonded NH stretching modes (Scheme 4).

3.2.1. Crystallinity calibration in the bulk state: amide stretching mode

It appears obviously that the crystallinity degree X_c depends on the infrared ν(C–C=O) band intensity in the amorphous and crystalline phases. We suggest to correlate X_c values obtained by DSC with the intensity of bands located at 922 and 936 cm^{-1} (for the amorphous and the crystalline phases, respectively), measured from PA bulk ATR spectra. The proposed equations, necessary to

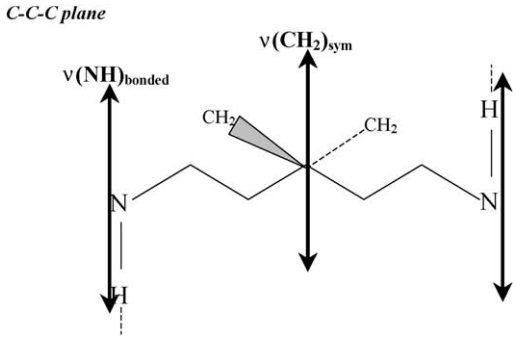

Scheme 4. Vibration modes direction of $\nu(NH)_{bonded}$ and $\nu(CH_2)_{sym}$.

establish such a relation, are the following

$$n_T^{CO} = n_{cr}^{CO} + n_{am}^{CO} = \frac{A_{cr}^{CO}}{\varepsilon_{cr}^{CO}} + \frac{A_{am}^{CO}}{\varepsilon_{am}^{CO}} \quad (3)$$

and

$$X_c = 1 - X_{am} = \frac{n_{cr}^{CO}}{n_T^{CO}} = \frac{n_{cr}^{CO}}{n_{cr}^{CO} + n_{am}^{CO}} \quad (4)$$

$$X_c = \frac{\frac{A_{cr}^{CO}}{\varepsilon_{cr}^{CO}}}{\frac{A_{cr}^{CO}}{\varepsilon_{cr}^{CO}} + \frac{A_{am}^{CO}}{\varepsilon_{am}^{CO}}} = \frac{A_{cr}^{CO}}{A_{cr}^{CO} + \frac{\varepsilon_{cr}^{CO}}{\varepsilon_{am}^{CO}} A_{am}^{CO}} \quad (5)$$

By considering the factor c equal to $\varepsilon_c/\varepsilon_{am}$, we obtain the following relation

$$X_c = \frac{A_{cr}^{CO}}{A_{cr}^{CO} + cA_{am}^{CO}} \quad (6)$$

where n_T^{CO} is the total number of CO moles; n_{cr}^{CO}, the number of CO moles in the crystalline phase; n_{am}^{CO}, the number of CO moles in the amorphous phase; A_{cr}^{CO}, the integrated band intensity of CO moles in the crystalline phase (at 936 cm^{-1}); A_{am}^{CO}, the integrated band intensity of CO moles in the amorphous phase (at 922 cm^{-1}); ε_{cr}^{C}, the molar absorption coefficient related to the ν(C–C=O) in the crystalline phase; ε_{am}^{CO}, the molar absorption coefficient related to the ν(C–C=O) in the amorphous phase; X_c, the crystallinity degree (%); X_{am}, the amorphous percentage; c is the resulting coefficient equal to $\varepsilon_c/\varepsilon_{am}$.

ε_c and ε_{am} were necessarily introduced since that the spectral response of any vibrator is dependent on its molar absorption coefficient which is a physical parameter related to the absorbing environment. Thus, we should consider two different coefficient: one for the vibrator in the crystalline phase (ε_c) and another one for the amorphous phase (ε_{am}).

For the calculation of coefficient c, the spectral decomposition of the ATR spectra in the 850–950 cm^{-1} region (Fig. 5) permits to obtain A_{cr} and A_{am}. By replacing these values in Eq. (6), it became possible to calculate c for each

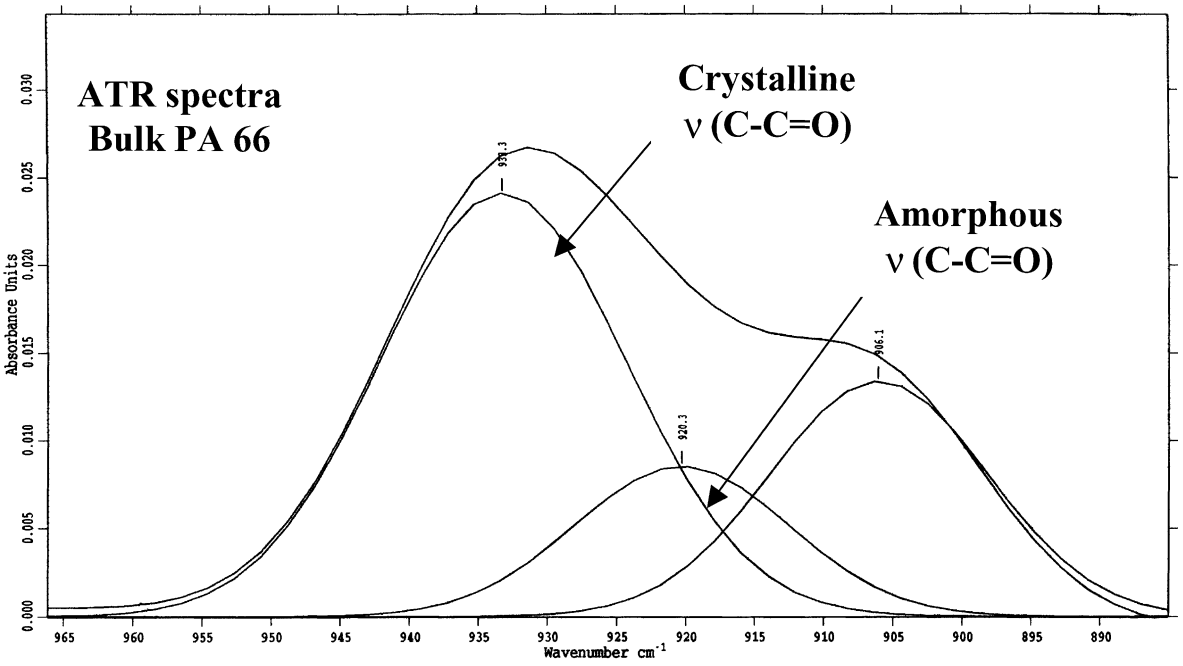

Fig. 5. Decomposition of the ATR spectra in the 850–950 cm^{-1} region for bulk PA66.

PA by considering X_c values obtained by DSC. Values of c are gathered in Table 4.

The crystallinity degree, for each PA, could then be expressed as:

$$X_c = \frac{A_{cr}^{CO}}{A_{cr}^{CO} + 4.5A_{am}^{CO}} \quad \text{for PA66} \tag{7}$$

$$X_c = \frac{A_{cr}^{CO}}{A_{cr}^{CO} + 3.6A_{am}^{CO}} \quad \text{for PA610} \tag{8}$$

$$X_c = \frac{A_{cr}^{CO}}{A_{cr}^{CO} + 3.1A_{am}^{CO}} \quad \text{for PA612} \tag{9}$$

We should mention that the decrease of the coefficient c is significant and shows how the absorption of CO groups involved in the crystalline phase decreases, with respect to those involved in the amorphous one, when the diacid aliphatic chain length increases.

3.2.2. Crystallinity calibration in the bulk state: NH and CH_2 stretching modes

Important differences are observed on the bulk PA66, 610 and 612 spectra. Spectral region of interest is the bonded NH absorption zone (Fig. 6).

Table 4
Calculated values of coefficient c ($c = \varepsilon_c/\varepsilon_{am}$)

PA	$c = \varepsilon_c/\varepsilon_{am}$
66	4.5
610	3.6
612	3.1

The spectral decomposition of these spectra in the 2750–3400 cm^{-1} region permits to obtain the band integrated intensity of the $\nu(CH_2)$ symmetric mode (noted $A(CH_2)s$) as well as the total bands integrated intensity of bonded NH modes (noted $A(NH)_{bonded}$). A linear relationship is found by plotting X_c, obtained by DSC, versus $A(NH)_{bonded}/A(CH_2)s$ (Fig.7).

This correlation has the equation

$$X_c = 0.919A(NH)_{bonded}/A(CH_2)s + 27.064 \tag{10}$$

and gives the value of X_c if $A(NH)_{bonded}$ and $A(CH_2)s$ are known.

The intersection of this line with the X_c axis gives a value equal to 27. This latter means that for $A(NH)_{bonded}$ equal to 0 the X_c is equal to 27. Theoretically, we could consider that in the absence of hydrogen bonds, we are in a polyethylene segments. Thus, a 27% crystallinity is related to the *trans–trans* conformations of CH_2 entities. This value is close to those of short polyethylene sequences (low to very low-density polyethylene).

In fact, PA adsorbed chains do not preserve the same conformations as in the bulk [44]. A rotation of the diacid/diamine planes (Scheme 5), previously observed (equal to 20°) [45], take into account the orientation contribution induced by the PA chain twist, in the $(NH)_{bonded}$ modes intensities, and in the CH_2 symmetric modes $(CH_2)s$. Thus, it was necessary to select the diacid CH_2 symmetric modes and NH bonded one, which even after the chain twist vibrate in the same direction.

But, in the bulk linear chain spectra, the diacid CH_2

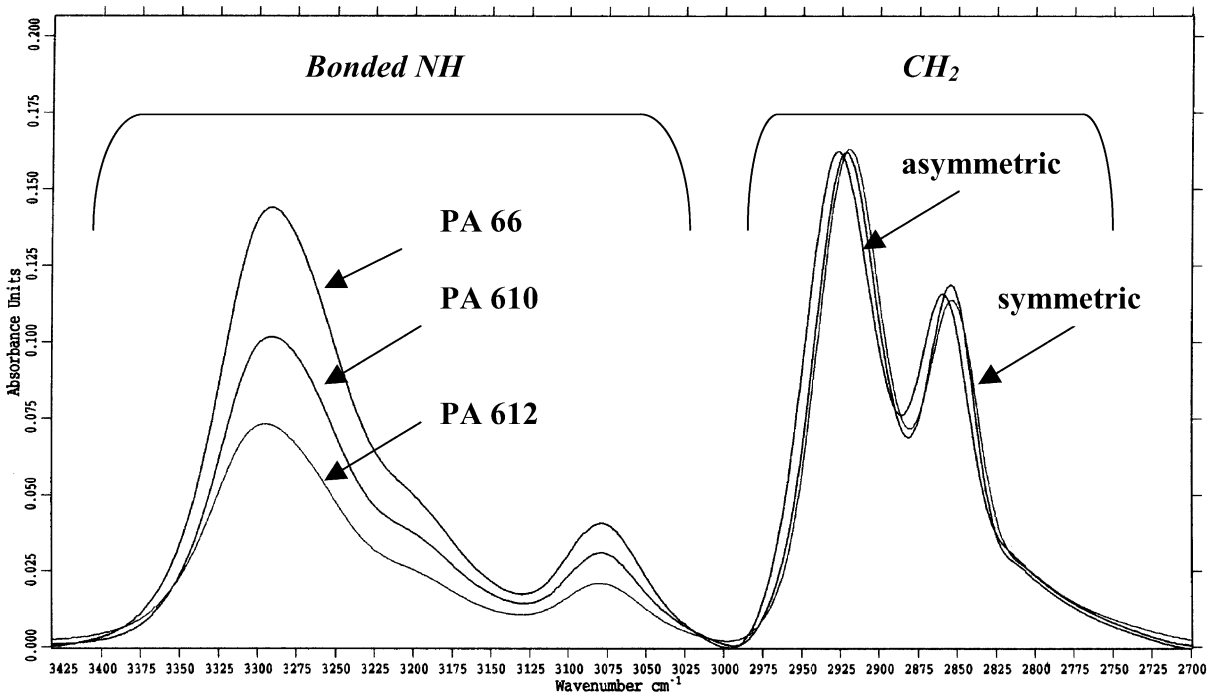

Fig. 6. Comparison of ATR spectra of bulks PA66, 610 and 612 in the 2700–3425 cm^{-1} zone.

symmetric modes response is not separated from the diamin one, and the measured intensity corresponds to the total symmetric modes (diacid plus diamin aliphatic carbons). Thus, we consider that, in the bulk case, $A(CH_2)s_{diacid}$ is related to $A(CH_2)s$ by a factor K which is equal to the ratio of N_{diacid} over the total aliphatic CH_2. K values are shown in Table 5.

For bulk spectra, $A(NH)_{bonded}$ is obtained by spectral integration between 3000 and 3400 cm^{-1}, while $A(CH_2)s_{diacid}$ is the multiplication of $A(CH_2)s$ by the factor K.

Fig. 8 shows that a linear evolution is obtained by plotting X_c versus $A(CH_2)s_{diacid}/A(NH)_{bonded}$.

This new relation, corrected from orientation effect in thin film, obey the equation

$$X_c = -54.044A(CH_2)s_{diacid}/A(NH)_{bonded} + 38.228 \qquad (11)$$

and will permit to estimate more precisely the X_c values.

These equations (Eqs. (3)–(11)) would be applied to the spin coated systems and their accuracy and limits will also be discussed.

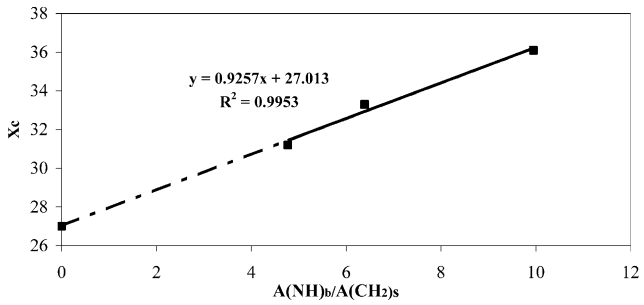

Fig. 7. Evolution of X_c versus $A(NH)_{bonded}/A(CH_2)s$.

3.3. Thin films analysis

3.3.1. IRRAS and PM-IRRAS

Films of 33 nm thick, as estimated by ellipsometry, were studied by IRRAS and PM-IRRAS. In Fig. 9, infrared spectra of PA66 thin film spin coated on gold substrate compared to the bulk one are represented.

In a recent work [44], we have discussed the structure, conformation and the orientation of spin coated PA. First, we have evidenced the stability of the crystalline structure of PA after adsorption, and second, conformational changes were revealed.

For thin film crystallinity measurements, we applied the previously described methods on different systems: gold and functionalized substrates.

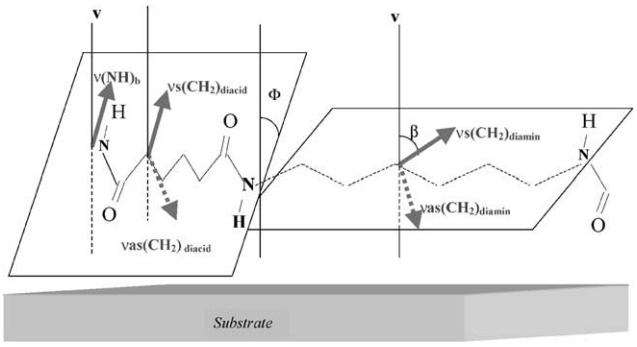

Scheme 5. Representation of PA chains twist.

Table 5
K values for PA66, 610 and 612

PA	N_{diacid}	N_{diamin}	$K = N_{diacid}/(N_{diacid} + N_{diamin})$
66	4	6	4/10
610	8	6	8/14
612	10	6	10/16

For these calculations (Eqs. (6) and (11)), one need to decompose IRRAS and PM-IRRAS spectra to obtain the integrated intensities, I_{cr} and I_{am}, of the ν(C–C=O) stretching mode (922 and 936 cm^{-1}) in thin films spectra, and also $I(NH)_{bonded}$, $I(CH_2)s$ and $I(CH_2)s_{diacid}$, from PM-IRRAS spectra.

We should mention that the decomposition in the 900–950 cm^{-1} region was not possible for all IRRAS and PM-IRRAS spectra due to the complexity of this region and its weak intensity (Fig. 9).

$I(NH)_{bonded}$ and $I(CH_2)s$ were obtained by PM-IRRAS spectra integration. In contrast, $I(CH_2)s_{diacid}$ could not be obtained directly from spectra, since the diamin and diacid CH_2 symmetric modes were not well resolved. It was then necessary to calculate this component from conformational parameters, such as ϕ and β (Scheme 5), defined as the tilt angles of, respectively, the diacid and diamin parts of the PA chains [44,45]. Application of PM-IRRAS selection rules permits to relate $I(CH_2)s_{diacid}$ and $I(CH_2)s$ as follows:

$I(CH_2)s_{diacid} \propto A(CH_2)s_{diacid}(\cos\theta\cos\phi)^2 \propto A(CH_2)sK(\cos\theta\cos\phi)^2$.
$I(CH_2)\ s_{diamin} \propto A(CH_2)\ s_{diamin}\ (\cos\theta\cos\beta)^2 \propto A(CH_2)\ sK'\ (\cos\theta\cos\beta)^2$.

And so

$$I(CH_2)s_{diacid} = \frac{I(CH_2)s}{1 + \dfrac{K'(\cos\beta)^2}{K(\cos\phi)^2}} \quad (12)$$

with $I(CH_2)s_{diacid}$, the diacid CH_2 symmetric mode integrated intensity corresponding to thin films; $A(CH_2)s_{diacid}$, the diacid CH_2 symmetric mode integrated intensity corresponding to the bulk; $A(CH_2)s$, the global CH_2 symmetric mode integrated intensity corresponding to the bulk; K is the ratio of diacid CH_2 number to the total CH_2. Values are shown in Table 5.

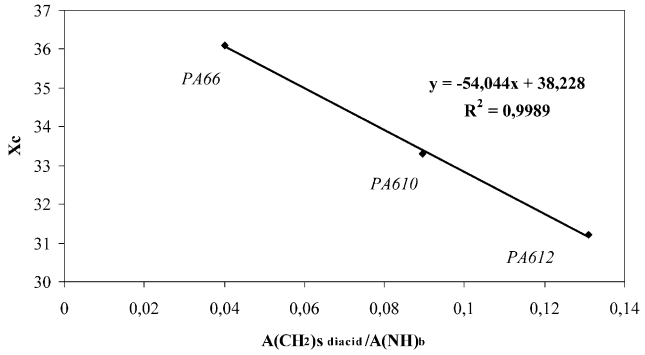

Fig. 8. Evolution of X_c versus $A(CH_2)s_{diacid}/A(NH)_{bonded}$.

Table 6
Calculated values of ϕ [45]

ϕ (°)	Gold substrates	NH_2 substrates	COOH substrates	OH substrates
PA66	40	41	40	41
PA610	41	43	44	42
PA612	43	43	40	41

$I(CH_2)s_{diamin}$: diamin CH_2 symmetric mode integrated intensity corresponding to thin films.
$A(CH_2)s_{diamin}$: diamin CH_2 symmetric mode integrated intensity corresponding to the bulk.
K': ratio of diamin CH_2 number to the total CH_2. Equal to 6/10, 6/14 and 6/16, respectively, for PA66, 610 and 612.
$I(CH_2)s$: global CH_2 symmetric mode integrated intensity corresponding to thin films.
θ: angle formed by the projection of the chain axis on the substrate plane.

The values of ϕ and β are shown in Tables 6 and 7, respectively, for PA66, 610 and 612 spin coated as thin films (33 nm) on gold substrates, or NH_2, COOH and OH functionalized substrates [45].

By replacing each parameter by its value, it became possible to reach X_c values from the proposed equations. Obtained X_c values, for each substrate, are gathered in Tables 8–11.

The comparison of these values indicates:

First, X_c magnitude increases due to substrate functionalization, and highest values are obtained for OH and COOH grafts.
Second, even in thin films, X_c decreases from PA66 to 612 whatever the substrate functionality.

Fig. 10 shows a comparison between thin films (Eq. (10)) and bulk X_c values.

As shown in Fig. 10, highest X_c values are obtained for OH and COOH grafts, which could means that these latter are very suitable seeds for PA crystallization. A lower effect is observed for NH_2 grafts. This observation could be explained by the magnitude of chain–grafts interactions and/or by the probability to establish these interactions. It

Table 7
Calculated values of β [45]

β (°)	Gold substrates	NH_2 substrates	COOH substrates	OH substrates
PA66	62	62	62	63
PA610	62	62	63	62
PA612	64	63	60	63

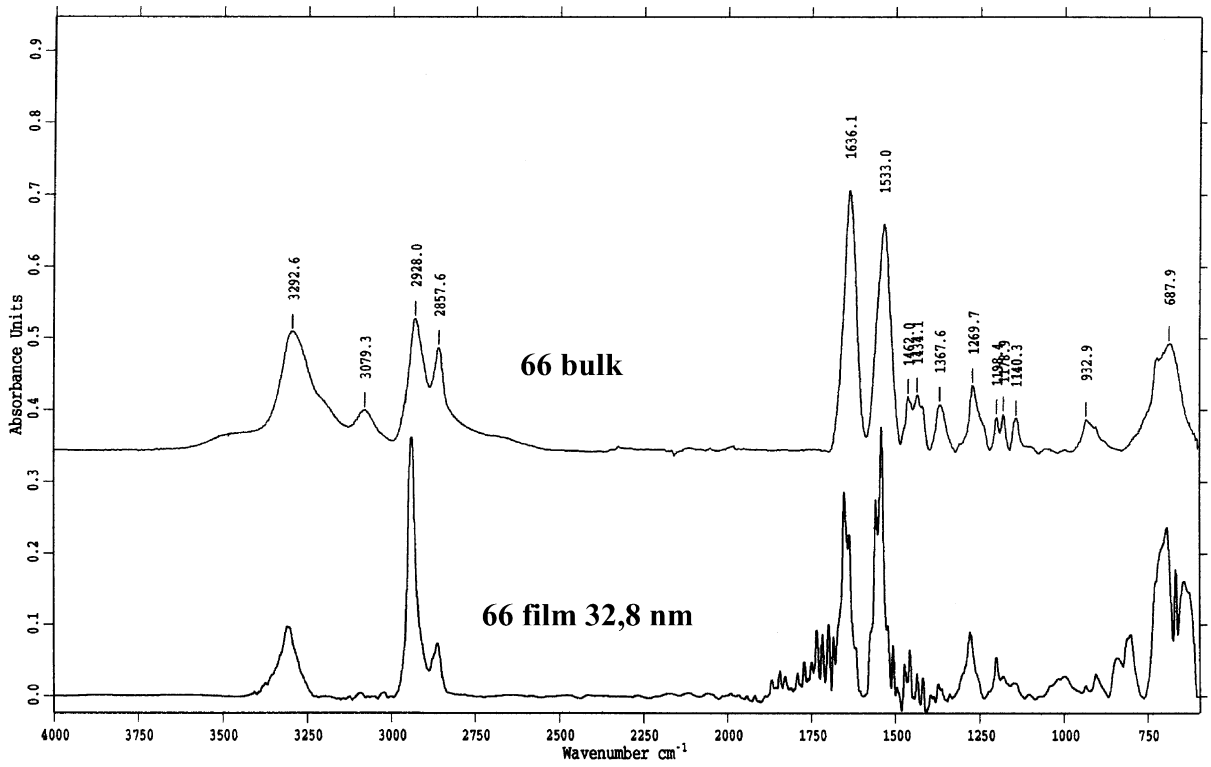

Fig. 9. ATR spectra of PA66 bulk compared with IRRAS spectra of its thin film adsorbed on gold substrate.

could be also due to a lower grafting density in the case of NH_2 molecules induced by the 4-aminothiophenol benzene units repulsion (high electronic density). The same argument can be used to justify the lower X_c values in the case of gold substrates. These latter present some surface contamination, and thus, very low heterogeneous seeds density (contamination particles) explains the low crystallinity degree measured. Therefore, we would compare, later in the paper, topographic images of gold and functionalized substrates in order to understand these crystallinity differences.

Fig. 10 also shows, as mentioned earlier, that the decreasing order of crystallinity, from PA66 to 612, is respected in the case of adsorbed films. A further look on IRRAS and PM-IRRAS spectra shows some differences in the wavenumber of CH_2 asymmetric stretching mode (Fig. 11). An

Table 8
X_c values of PA66, 610 and 612, adsorbed on gold coated substrates, as obtained by IRRAS (for Eq. (6)) and PM-IRRAS (Eqs. (10) and (11))

PA	Bulk; X_c (DSC)	Gold substrates		
		X_c (Eq. (6))	X_c (Eq. (10))	X_c (Eq. (11))
66	36.1	32.9	33.7	32.5
610	33.3	30.6	31.8	30.6
612	31.2	29.9	29.6	28.3

Table 9
X_c values of PA66, 610 and 612, adsorbed on NH_2 functionalized substrates, as obtained by PM-IRRAS (Eqs. (10) and (11))

PA	Bulk; X_c (DSC)	NH_2 substrates		
		X_c (Eq. (6))	X_c (Eq. (10))	X_c (Eq. (11))
66	36.1	–	36.9	35.8
610	33.3	–	35.4	33.5
612	31.2	–	33.5	31.4

Table 10
X_c values of PA66, 610 and 612, adsorbed on COOH functionalized substrates, as obtained by PM-IRRAS (Eqs. (10) and (11))

PA	Bulk; X_c (DSC)	COOH substrates		
		X_c (Eq. (6))	X_c (Eq. (10))	X_c (Eq. (11))
66	36.1	–	38.1	36.4
610	33.3	–	36.1	34.2
612	31.2	–	35.3	33.2

Table 11
X_c values of PA66, 610 and 612, adsorbed on OH functionalized substrates, as obtained by IRRAS (Eq. (6)) and PM-IRRAS (Eqs. (10) and (11))

PA	Bulk; X_c (DSC)	OH substrates		
		X_c (Eq. (6))	X_c (Eq. (10))	X_c (Eq. (11))
66	36.1	37.2	38.2	36.4
610	33.3	35.3	36.3	34.6
612	31.2	32.7	35.6	33.4

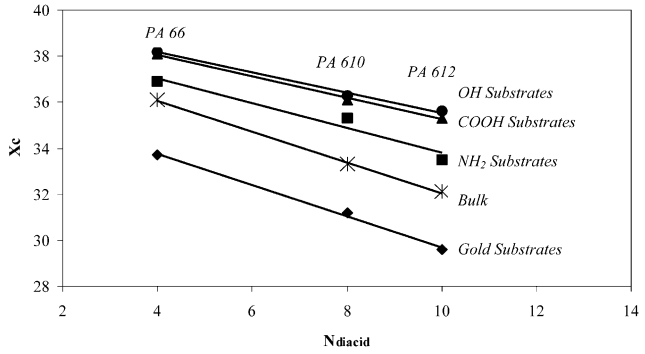

Fig. 10. Comparison of X_c values of PA: bulk and thin films.

important fact is the splitting of the $\nu_{as}(CH_2)$ in two contribution, the first one located at 2920 cm^{-1} and the second one at 2938 cm^{-1}.

The shift of the component at 2938 cm^{-1} to lower wavelength for PA610 and 612 with respect to the PA66 (2939, 2937 and 2936 cm^{-1}, respectively, for PA66, 610 and 612), has already been related to the decrease of the average number of *trans* conformation (compared to *gauche* one) of C–C–C sequences [46]. This means that the average density of *gauche* conformations relative to *trans* one increases from PA66 to 612. So, spin coated PA612 and 610 are less crystalline than PA66. This observation is in good agreement with X_c calculated values.

3.3.2. AFM

Topographic AFM images (Fig. 12) reveal great differences between the studied substrates. Dense structures of reduced spatial extension are observed for OH and COOH grafts, while big spherulitic and less dense structures are identified for NH_2 and gold substrates. Even if these images are obtained in the surface plane and not in three dimensions, we could conclude that the high crystalline density observed in case of OH and COOH substrates confirms their highest X_c values. Observed structures for these two cases imply apparently a high nucleation density compared to NH_2 substrates, where spherulitic growth is favored (spherulitic radius of 10 μm and more). In this case (NH_2 grafts), we could also attribute these observations to the lower grafting density induced by the repulsion forces between grafted molecules as mentioned earlier. Gold substrate seems to induce, in some case, a spherulitic morphology probably due to surface contamination acting as surface seeds.

4. Conclusion

In this work, we propose an original method for the determination of thin film crystallinity degree by using infrared spectroscopy. Two methods, calibrated from the bulk state, were proposed.

The first one based on the splitting of the ν(C–C=O) vibrator into two different wavenumber depending on its physical state: 922 cm^{-1} for the amorphous phase and 936 cm^{-1} for crystalline one. We suggest a relationship involving the intensities of these signals and a coefficient

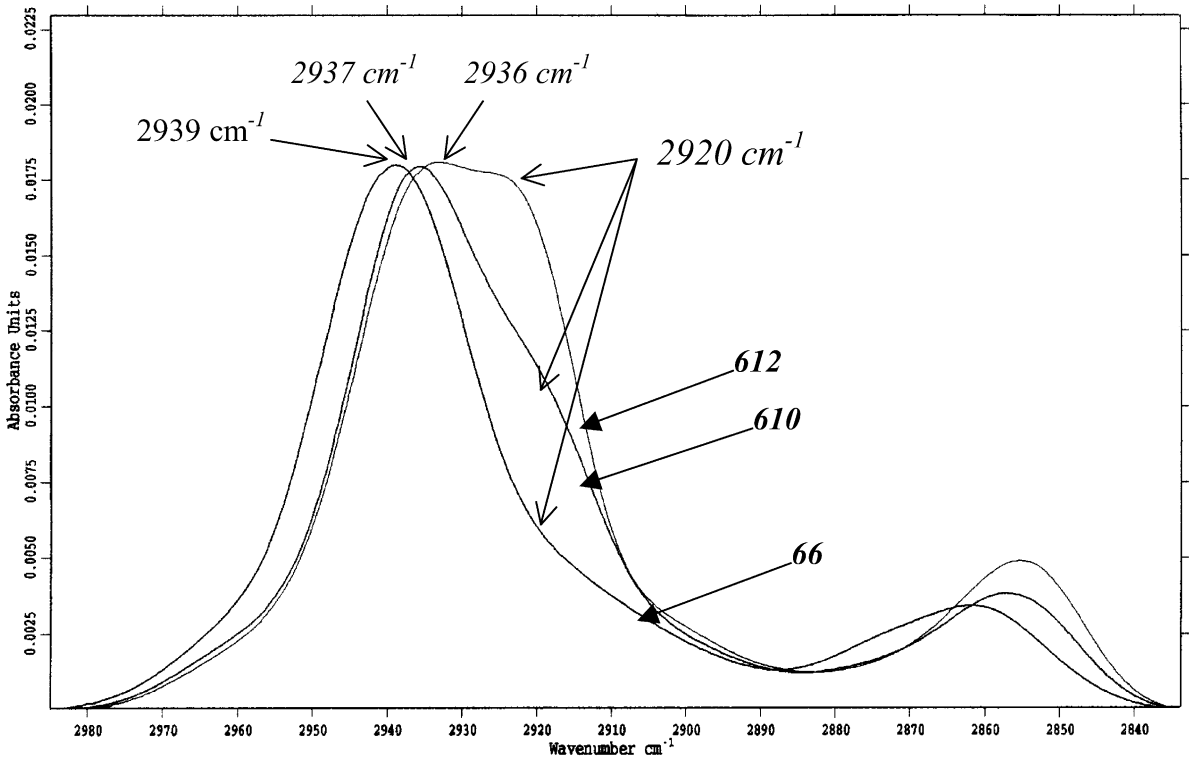

Fig. 11. Representation of the 2700–3000 cm^{-1} region for 66, 610 and 612 thin films on OH functionalized substrates.

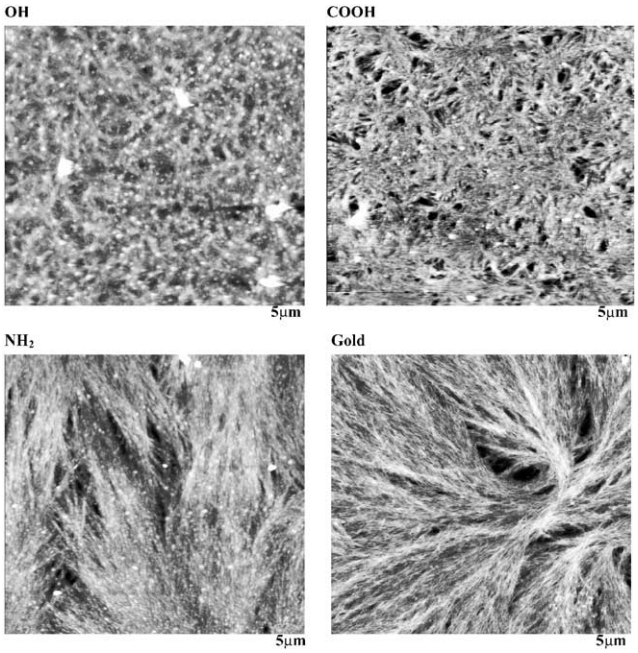

Fig. 12. Comparison of PA66 adsorbed on OH, COOH, NH_2, and gold substrates.

c, related to the vibrator absorption coefficients ε_c and ε_a, respectively, for the crystalline and amorphous phases. This method was applied to adsorbed systems, but the limitation of its application was determined by the spectral quality in the 600–1000 cm^{-1} region that has a low signal in the IRRAS and PM-IRRAS spectra.

The second method is based on quantitative analysis of two other vibrators: the bonded NH stretching mode $\nu(NH)_{bonded}$ and the CH_2 symmetric stretching modes $\nu(CH_2)$s. The choice of symmetric modes was done to reduce the orientation contribution in adsorbed systems, since that, for linear PA chains, the CH_2 symmetric modes vibrate in the same direction of the NH stretching mode. But change of conformation [44,45] in the adsorbed state impose a correction of this method by considering only the diacid CH_2 stretching mode that, even after the chain twist, vibrate in the same direction of the $\nu(NH)_{bonded}$.

Our calculations, based on these two methods, show a preferential PA thin films crystallization phenomena on functionalized substrates. We attribute these results to the fact that chemical grafts are acting as nucleation seeds. Furthermore, highest crystallinity degrees were found for OH and COOH grafts that implies a high grafting density of their molecules with respect to the NH_2 substrates. AFM topographic analyses are in good agreement with X_c calculated values and show a highest PA thin films lamellae density for OH and COOH substrates relative to gold and NH_2 ones.

References

[1] Chen YK, Kukureka SN, Hooke CJ, Rao M. J Mater Sci 2000;35:1269.
[2] Jones NA, Atkins EDT, Hill MJ. J Polym Sci 2000;38:1209.
[3] Vasanthan N, Salem DR. J Polym Sci 1999;38:516.
[4] Ramesh C. Macromolecules 1999;32:5704.
[5] Murthy NS, Wang ZG, Hsiao S. Macromolecules 1999;32:5594.
[6] Smith RL, Fang Z, Inomata H, Arai K. J Appl Polym Sci 1999;76:1062.
[7] Ramesh C. Macromolecules 1999;32:3721.
[8] Vasanthan N, Murthy NS, Bray RG. Macromolecules 1998;31:8433.
[9] Guoming W, Deyue Y. Chin J Polym Sci 1998;16:241.
[10] Young TH, Lin DJ, Gau JJ, Chuang WY, Cheng LP. Polymer 1998;40:5011.
[11] Muellerleile JT, Freeman JJ, Middleton JC. J Appl Polym Sci 1997;69:1675.
[12] Itoh T, Ishikawa H, Hashimoto M. J Phys Soc Jpn 1997;66:2726.
[13] Asano T, Calleja FJB, Giri L, Yoshida T, Miyashita N, Matsuura M, Kitabatake J, Hatanaka I, Seri K. J Macromol Sci 1997;B36:799.
[14] Navarro E, Subirana A, Puiggali J. Polymer 1996;38:3429.
[15] Gonsalves KE, Mungara PM. Trends Polym Sci 1996;4:25.
[16] Radusch HJ, Stolp M, Androsch R. Polymer 1994;35:3568.
[17] Ramesh C, Keller A, Eltink SJEA. Polymer 1994;35:2483.
[18] Atkins EDT, Hill M, Hong SK, Keller A, Organ S. Macromolecules 1992;25:917.
[19] Dreyfuss P, Keller A. J Polym Sci 1973;11:193.
[20] Jakes J, Krimm S. Spectrochim Acta 1971;27A:19.
[21] Dreyfuss P, Keller A. J Macromol Sci 1970;B4:811.
[22] Koenig JL, Agboatwalla MC. J Macromol Sci, Phys 1968;B2:391.
[23] Bunn CW, Garner EV. Proc R Soc Lond 1947;A189:393.
[24] Mathot VBF. Calorimetry and thermal analysis of polymers. Hanser Publishers, 1994.
[25] Mo Z, Yang B, Zhang H. Anal Sci 1991;7:1637.
[26] Polizzi S, Fagherazzi G, Benedetti A, Battagliarin M. Eur Polym J 1991;27:85.
[27] Long Y, Shanks RA, Stachurski ZH. Prog Polym Sci 1995;20:651.
[28] Armistead K, Goldebeck-Wood G. Adv Polym Sci 1992;100:219.
[29] Porter MD, Bright TB, Allara DL, Chidsey CED. J Am Chem Soc 1987;109:3559.
[30] Porter MD. Anal Chem 1988;60:1143A.
[31] Troughton EB, Bain CD, Whitesides GM, Nuzzo RG, Allara DL, Porter MD. Langmuir 1988;4:365.
[32] Yen YS, Wong JS. J Phys Chem 1983;93:7208.
[33] Dowry AE, Marcott C. Appl Spectrosc 1982;36:414.
[34] Golden WG, Saperstein DD. J Electron Spectrosc Relat Phenom 1983;30:43.
[35] Golden WG, Saperstein DD, Severson MW, Overend J. J Phys Chem 1984;88:572.
[36] Pang KP, Benziger JB, Soriaga MP, Hubbard AT. J Phys Chem 1984;88:4583.
[37] Golden WG, Kunimatsu K, Seki H. J Phys Chem 1984;88:1275.
[38] Golden WG. Fourier Transform Infrared Spectrosc 1985;4:315.
[39] Buffeteau T, Desbat B, Pézolet M, Turlet JM. J Chim Phys 1993;90:1467.
[40] Buffeteau T, Desbat B, Devaure J, Salimi A, Turlet JM. J Chim Phys 1993;90:1871.
[41] Brill RJ. J Prakt Chem 1942;161:49.
[42] Buffeteau T, Desbat B, Turlet JM. Appl Spectrosc 1991;45:380.
[43] Hummel DO. Infrared spectra of polymers. New York: Wiley, 1966.
[44] Elzein T, Brogly M, Castelein G, Schultz J. J of Polymer Sci. Part B: Polymer physics, 2002, vol. 40, in press.
[45] Elzein T, Brogly M, Schultz J. Submitted for publication.
[46] Snyder RG. J Chem Phys 1967;47:1316.